sections and CH_3NC quantum yield can be extrapolated with confidence to atmospheric pressure to model the photochemical removal of MITC in the atmosphere. Experiments should be carried out to determine the importance of additional MITC removal pathways, such as reaction with OH, to gain a more complete understanding of its fate.

The persistence, fate, and health consequences of CH_3NC should also be examined because it is the principal stable MITC photodegradation product at solar wavelengths. Because CH_3NC does not absorb light with $\lambda > 260$ nm ($\sigma < 10^{-21}$ cm^2) (*23*), it is stable with respect to photolysis in the troposphere. At present, no toxicological data exist for CH_3NC; it has an unpleasant odor and is thought to behave like CO in binding to hemeproteins (*24*). The transformation of CH_3NC to CH_3NCO has been observed in laboratory photolysis studies of MITC in the presence of O_2 (*25*) and is adequately described by the photo-oxidation of CH_3NC by SO_2. Although this mechanism does not apply under atmospheric conditions because SO_2 does not build up to sufficiently high levels, the reaction of CH_3NC with O_3, NO_x, or HO_2 might result in production of the highly toxic (*26*) CH_3NCO. The conversion of alkyl isocyanides to isocyanates by O_3 (*27*) and NO (*28*) has been observed in solution. Laboratory studies on the chemistry of CH_3NC, along with accurate field measurements of MITC, CH_3NC, and CH_3NCO concentrations, are thus needed to adequately assess the health risks resulting from the agricultural use of metam-sodium.

REFERENCES AND NOTES

1. Nihon Schering K. K. and Shionogi and Co., Ltd., *J. Pestic. Sci.* **15**, 297 (1990).
2. "Fumigants and nematicides," in *Chemical Economics Handbook* (SRI International, Palo Alto, CA, 1993).
3. J. C. Robinson and W. S. Pease, *California Policy Seminar Brief 5* (1993).
4. M. Leistra and S. J. H. Crum, *Water Air Soil Pollut.* **50**, 109 (1990).
5. F. van den Berg, *Atmos. Environ. Part A* **27**, 63 (1993).
6. "Ambient Air Monitoring in Contra Costa County During March 1993 After an Application of Metam-Sodium to a Field" (California Air Resources Board, Monitoring and Laboratory Division, Sacramento, CA, 1993).
7. M. J. DiBartolomeis *et al.*, "Evaluation of the Health Risks Associated with the Metam Spill in the Upper Sacramento River" (Office of Environmental Health Hazard Assessment, California Environmental Protection Agency, Berkeley, CA, 1992).
8. J. Heicklen, *Atmos. Environ.* **16**, 821 (1982).
9. S.-C. Woo and T. C. Chu, *J. Chin. Chem. Soc.* **5**, 162 (1937); C. N. R. Rao, J. Ramachandran, S. Somasekhara, *Curr. Sci.* **27**, 474 (1958); E. Svatek, R. Zahradnik, A. Kjaer, *Acta Chem. Scand.* **13**, 442 (1959).
10. P. D'Amario, G. DiStefano, M. Lenzi, A. Mele, *J. Chem. Soc. Faraday Trans. 1* **68**, 940 (1972).
11. I. Tokue, A. Hiraya, K. Shobatake, *Chem. Phys.* **117**, 315 (1987).
12. F. J. Northrup and T. J. Sears, *J. Chem. Phys.* **93**, 2337 (1990).
13. I. Tokue, K. Kobayashi, T. Honda, Y. Ito, *J. Phys. Chem.* **94**, 3485 (1990).
14. R. Holland, D. W. G. Style, R. N. Dixon, D. A. Ramsay, *Nature* **182**, 336 (1958).
15. J. E. Nicholas and C. A. Amodio, *J. Chem. Soc. Faraday Trans. 1* **76**, 1669 (1980).
16. U. Schmidt, K. Kabitzke, I. Boie, C. Osterroht, *Chem. Ber.* **98**, 3819 (1965); R. Jahn and U. Schmidt, *Monatsh. Chem.* **109**, 161 (1978).
17. B. J. Finlayson-Pitts and J. N. Pitts, *Atmospheric Chemistry: Fundamentals and Experimental Methods* (Wiley, New York, 1986), p. 134.
18. R. A. Alvarez and C. B. Moore, *J. Phys. Chem.*, in press.
19. H. W. Thompson and R. L. Williams, *Trans. Faraday Soc.* **48**, 502 (1952).
20. C. R. Boxall and J. P. Simons, *J. Photochem.* **1**, 363 (1972–73).
21. O. P. Strausz, in *Sulfur in Organic and Inorganic Chemistry*, A. Senning, Ed. (Dekker, New York, 1972), vol. 2, chap. 11; D. D. Davis and R. B. Klemm, *Int. J. Chem. Kinet.* **5**, 841 (1973).
22. J. G. Calvert and J. N. Pitts, *Photochemistry* (Wiley, New York, 1967), p. 584.
23. B. K. Dunning, D. H. Shaw, H. O. Pritchard, *J. Phys. Chem.* **75**, 580 (1971).
24. H. M. Walborsky and M. P. Periasamy, in *The Chemistry of Functional Groups, Supplement C*, S. Patai and Z. Rappoport, Eds. (Wiley, New York, 1983), p. 836.
25. J. D. Geddes and G. C. Miller, unpublished results; R. A. Alvarez, thesis, University of California at Berkeley (1993).
26. The Occupational Safety and Health Administration's 8-hour Permissible Exposure Level (PEL) is 20 ppb (Sigma/Aldrich Material Safety Data Sheet on CD-ROM, revision 2.14).
27. H. Feuer, H. Rubinstein, A. T. Nielsen, *J. Org. Chem.* **23**, 1107 (1958).
28. T. Saegusa, S. Kobayashi, Y. Ito, *Bull. Chem. Soc. Jpn.* **43**, 275 (1970).
29. D. F. Bezuidenhout, in *Handbook of Optical Constants of Solids*, E. D. Palik, Ed. (Academic Press, San Diego, CA, 1991), p. 831.

30. The authors thank G. C. Miller for pointing out that CH_3NCO could be formed in this system. This work was supported by the Director, Office of Energy Research, Office of Basic Energy Sciences, Chemical Sciences Division of the U.S. Department of Energy, under contract DE-AC03-76SF0098.

19 August 1993; accepted 16 November 1993

Structure of Solidified Colloidal Array Laser Filters Studied by Cryogenic Transmission Electron Microscopy

Eduardo A. Kamenetzky,* Lino G. Magliocco, Hans P. Panzer

Ordered arrays of charged uniform colloidal polystyrene particles in solution form a single-wavelength laser filter that is transparent to other wavelengths. A usable filter was prepared by solidification within an acrylamide–methylene-bisacrylamide gel. The rejection wavelength of the colloidal array filter changes with gel composition. Cryogenic transmission electron microscopy of two gel formulations shows that the colloidal array filter is composed of AAA stacking of close-packed planes. Excellent agreement is found between the layer spacings measured and those predicted from the rejection wavelengths.

Suspensions of highly charged colloidal particles (polyballs) or macromolecules form crystalline arrays at particular regions of a ternary phase diagram whose locations depend on particle concentration, counterion concentration, and temperature (*1, 2*). Many naturally occurring colloidal crystalline arrays exist, for example, certain viruses, opal crystals, and solutions of macroions, proteins, cells, ionic micelles, and polynucleotides (*3, 4*). Polyball suspensions are a unique model system for understanding the behavior and stability of real colloidal dispersions (*5*). They also constitute a well-understood experimental system that can be used to model three-dimensional (3D) and two-dimensional (2D) phase transitions in quiescent and sheared crystals (*3, 6*). Polyball colloidal crystals can also function as optical wavelength rejection filters (*7*).

However, colloidal array filters (CAF) in aqueous suspensions have very limited temperature and mechanical stability. Freezing destroys CAFs, high temperature causes the crystalline array to melt, and mechanical shock destroys particle ordering. To produce potentially practical filters, we need a way of solidifying a CAF while preserving its optical properties. Recently, an intermediate step toward a solid CAF was demonstrated: solidification of the suspension within a gel (*8*). The structures of these solidified CAFs were studied by cryogenic transmission electron microscopy (CTEM) (*9*).

There are many potential applications for solidified CAFs in the fields of laser medicine, laser spectroscopy, and laser eye protection. Two CAF properties that are of particular interest are their transmittance of <1% at the rejection wavelength and a narrow bandwidth ≈20 nm. It is thus possible to reject a single wavelength while observing the remainder of the visible spectrum. For example, a surgeon could use a laser, spot its precise location, and at the

CYTEC Research and Development, 1937 West Main Street, P.O. Box 60, Stamford, CT 06904.

*To whom correspondence should be addressed.

same time observe the patient and symptomatology with little intensity and color distortion. In spectroscopy, the filters would be particularly useful for optical techniques where the intensity of the analyzed signal is weak compared to the intensity of the exciting beam, for example, in Raman spectroscopy (*7*).

Monodispersed electrically charged latex particles are prepared by the copolymerization of styrene with sulfonic acid co-monomers. The latex particle size is ≈100 nm, and the surface charge is ≈20,000 charges per particle or more (Fig. 1). The primary force between particles is then a repulsive long-range Coulombic interaction. Minimization of electrostatic repulsive interactions results in the formation of crystalline structures. The CAF consists of a stack of layers (spacing *d*), which show hexagonal close-packing of the latex particles (spacing d_n) (Fig. 1). The colloidal array acts as a filter by virtue of the Bragg diffraction of the incident laser at normal incidence. The spacing *d* can be of the order of several sphere diameters and is in the range of the wavelength of visible light. Formation of a solid filter requires embedding of the 3D colloidal array in an optically clear gel. A self-supporting film was made by in situ polymerization of an acrylamide–methylene-bisacrylamide (AMD-MBA) gel (Fig. 1). The absorbance and narrow bandwidth that are obtained with a few hundred planes of colloidal particles result in devices with excellent filter properties (*10*).

Two solidified CAFs were selected for CTEM study. These two filters were prepared from a poly[styrene-*co*-(sodium 1-allyloxy-2-hydroxypropane sulfonate)] latex with an average particle diameter of 107 nm, a polydispersity index of 1.039, and surface charge density of 9.21 μC/cm² (*8*). The colloidal arrays were solidified within an AMD-MBA gel matrix. The two gel compositions were 19:1 and 9:1 AMD:MBA. Solutions of the gel monomers and ordered latex were mixed and cleaned over ion-exchange resin. The latex in the mixture forms an ordered colloidal array, as shown by diffraction experiments. The solidification process is designed to lock the colloidal array into a 3D network without affecting its order. Photoinitiation of radical polymerization with ultraviolet (UV) light in the presence of multifunctional monomers results in the rapid formation of a cross-linked polymer network under mild conditions. Solutions of AMD-MBA gel into loose networks when polymerized at low temperatures after a 10-min exposure to UV radiation. The supernatant ordered mixture was injected between quartz plates 125 to 175 μm apart. The injection process produced shear-induced structures that were, however, still crystalline. Because typical relaxation times of these shear-induced structures (*2*) are greater than several hours and much greater than the polymerization time, the crystalline structure of the CAF is that induced by shear of the supernatant ordered mixture (*8*). Filters solidified in 19:1 AMD:MBA gel had a rejection wavelength of 550 ± 4 nm, a bandwidth of 19 ± 1.4 nm, and a transmittance of 0.83 ± 0.04%, whereas filters solidified in 9:1 AMD:MBA gel had a rejection wavelength of 507 ± 3 nm, a bandwidth of 23 ± 5 nm, and a transmittance of 0.22 ± 0.02%.

For TEM specimen preparation, a thick uniform layer of polyacrylamide was polymerized onto both surfaces of the CAF film (total thickness, ≈900 μm). The TEM samples were obtained from these layered structures. The CAF containing ~80% water was cryoprotected by the infusion of a solution of 2.3 M sucrose and 0.1 M $NaPO_4$ for 24 hours. This solution is used routinely for cryoultramicrotomy of biological structures (*11*). The cryogenic specimens were free of freezing damage and had the required plasticity for thin-sectioning. The TEM technique described here is applicable only to solidified CAFs; for liquid colloidal arrays, a freeze-fracture and replication electron microscopy method has been used recently (*12*).

Cryoultramicrotomy was performed with a Reichert-Jung (Deerfield, Illinois) FC4E instrument. The sample was placed on a clamping holder for low-elasticity samples and then cooled in the cryochamber to −85°C when it was shaped. The best conditions for 0.3-μm-thick sections were obtained at −85°C, slow sectioning speed, and no floating medium. The sections, on a support grid, were transferred to a Philips 420 TEM with a Gatan 626 cryo-transfer holder. The specimen temperature during transfer remained below −85°C at all times. The spacings *d* and d_n are the average of 40 measurements obtained by image analysis with a PGT IMIX system (Princeton Gamma Tech). We analyzed the areas that were free of crystalline defects. Because the error of measurement of a spacing over several lattice planes is small, the standard deviation of the spacings represents mostly the paracrystalline distortion of the colloidal array.

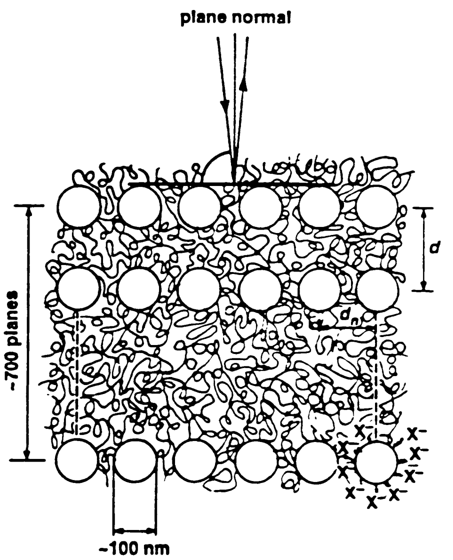

Fig. 1. Schematic of a CAF. The operating principle of the device is Bragg diffraction of a laser beam at normal incidence to the plane of the filter. The crystalline arrangement of the monodispersed polystyrene spheres embedded in an AMD-MBA gel is shown. The functionality of the spheres is indicated by X^- in the lower right corner. The size of the spheres and the interlayer and interparticle spacings *d* and d_n are in the range of wavelengths of visible lasers and can be tailored by processing of the CAFs.

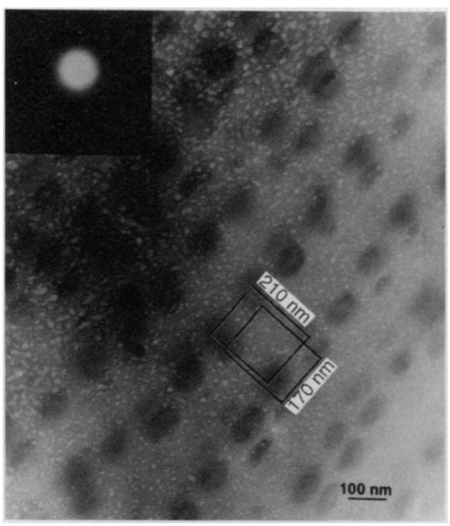

Fig. 2. A CAF in 19:1 AMD:MBA. The close-packed planes have AAA stacking (*13*) with an interplanar spacing of 210 nm. (**Inset**) The SAD pattern of the matrix.

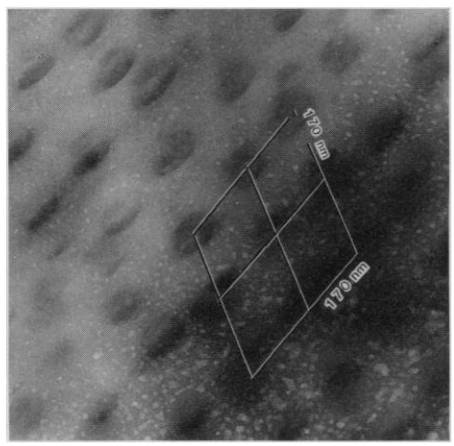

Fig. 3. A CAF in 19:1 AMD:MBA. Arrangement of polyballs in the close-packed planes.

The spacing between close-packed planes in the CAF in 19:1 AMD:MBA (Fig. 2) is 210 ± 15 nm. The equation for Bragg diffraction of CAFs at normal incidence is (10)

$$\lambda_o = 2nd \quad (1)$$

where λ_o = the rejection wavelength maximum in air, n = 1.333 is the measured refractive index of the matrix, and d is the spacing of the refracting planes. The predicted rejection wavelength, 560 nm, agrees well with the observed maximum rejection wavelength, 550 nm. From the spacings of the close-packed planes, we conclude that the CAF consists of about 700 planes of colloidal particles.

The selected-area diffraction (SAD) pattern (Fig. 2, inset) revealed that the matrix in all samples was amorphous and free from ice crystals. The close-packed planes in Fig. 2 are seen twice because of the angle of the thin section. For the same reason, only a cap of the spherical particles is observed. However, the size of the caps corresponds to 100-nm-diameter polystyrene-sulfonate particles.

The particle arrangement in the close-packed planes (Fig. 3) has the sixfold symmetry that corresponds to {111} planes in face-centered-cubic (fcc) and hexagonal close-packed (hcp) structures. The nearest neighbor distance d_n is 170 ± 15 nm. Both micrographs (Figs. 2 and 3) show some disorder, which is expected because of the deviation from an ideal monodispersed size distribution and unequal charge distribution in the polystyrene-sulfonate particles. The stacking of the close-packed planes is AAA (13).

The crystalline structure of the close-packed planes in the CAF of a 9:1 AMD:MBA gel (Fig. 4) also shows sixfold symmetry. The nearest neighbor distance is d_n = 150 ± 15 nm. The AAA stacking sequence of close-packed planes (Fig. 5) has a layer d = 185 ± 17 nm. The predicted rejection wavelength is 493 nm, and the difference between the observed and predicted rejection wavelength is only 3%. In CAFs, grain boundary planes should be normal to the close-packed planes. A triple grain boundary junction is illustrated in Fig. 6; the {010} planes are shown with the disorder occurring at the grain boundaries.

That the CAF consists of a stacking of hcp planes is expected from the structure of concentrated latex dispersions under shear (14–16). The solidified CAF is produced by rapid polymerization of an ordered array injected into a narrow cavity between two quartz plates. Concentrated suspensions of monodispersed colloids in a Newtonian fluid show ordered hcp layer structures under a wide variety of shear rates (14, 16). The colloids reside in layers that are parallel with surfaces of constant shear, and the direction of close-packing is parallel to the flow vector. A hexatic structure that displays extended correlations in the orientation of hexagonal clusters of particles, but has an exponential decay (with shear rate) of translational order, has been observed as an intermediate structure between quiescent crystalline colloidal arrays and colloidal liquid disordered structures (17). In dilute solutions, the 2D close-packed layers slip freely past each other (18). Even for disordered colloidal fluids, layering has been induced by parallel glass walls (19). Neutron scattering experiments show that at intermediate shear rates, there is an in-plane shear, which results in string-like displacements along the velocity vector but maintains a dynamical fcc registration between planes (1, 18, 20).

Other experiments were reported with conditions similar to those studied here: 128-nm spheres, 100- to 300-μm spacing between cell walls, and volume fractions of 5.5 to 15.4% (21). Measurements of the rejection wavelength of these samples indicate a maximum expansion of the layer spacing of 2% when the sample is under shear; for larger polyballs 497 nm in diameter, the maximum expansion is 10% (21). At the same time, the close-packed distance within the layers decreases (21). Finally, experimental evidence shows that phase transitions involving stack type and stacking sequences occur as a change from 3D packing to 2D behavior occurs (22).

None of the experiments mentioned above is expected to be a complete representation of the complex microstructure development in the CAFs described here. The fact that solidified CAFs obtained shortly after injection show a well-developed rejection peak indicates that the structure of the CAF is the one that develops under the shear necessary to inject the materials. We confirmed this by obtaining Kossel ring patterns before and after polymerization. The patterns were practically identical, showing that solidification by polymerization of a gel matrix had little effect on crystal structure. The Kossel rings showed hexagonal symmetry.

One important point in the discussion of the structure of the solidified CAFs is the observed volume percentage of polyballs. The observed volume fraction in the 9:1 AMD:MBA CAF was 12.2%, and the corresponding fraction in the mixture used to produce the filter was 8.4%. The observed volume fraction in the 19:1 AMD: MBA CAF was 10.6%, and the corresponding fraction in this formulation was 8.6%. Thus, the CAFs show a contraction from an ideal volume-filling crystal. This phenomenon has been studied in detail by others (2, 4, 23). Regions of order and disorder coexist in what is termed a two-state structure (2, 4, 23). The size of the ordered regions increases with time by Ostwald ripening. It takes several months for the colloidal crystals to reach millimeter size (24). Our results show that the grain boundaries are normal to the plane of the CAF. This implies that each crystallite is oriented in a layered structure by the shear flow. Thus, when diffraction

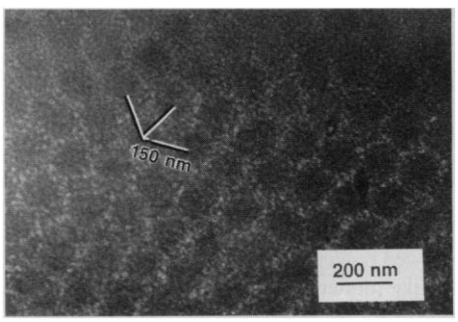

Fig. 4. A CAF in 9:1 AMD:MBA. Arrangement of polyballs in the close-packed planes.

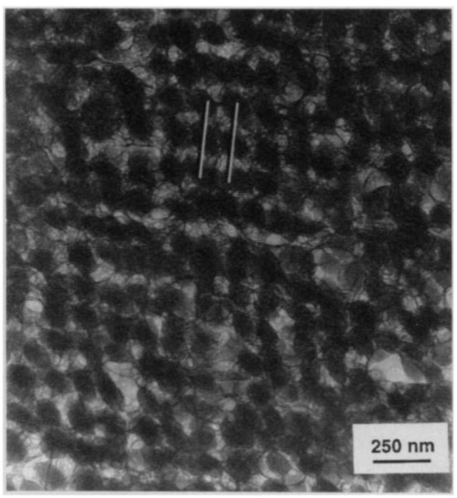

Fig. 5. A CAF in 9:1 AMD:MBA. AAA stacking of close-packed planes.

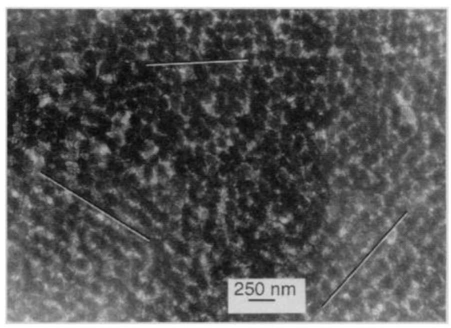

Fig. 6. Triple grain boundary junction in a CAF in 9:1 AMD:MBA. A close-packed direction in each crystal is indicated.

properties are measured at normal incidence, the CAF looks like a single crystal. A further implication of colloidal crystal contraction is that there must be a net attractive force at fixed interparticle distance (2, 4).

The choice of AMD-MBA gels as the matrix in the intermediate step of CAF solidification is, in many respects, a good one. For low-volume fractions, the monomer does not prevent the diffusion necessary for crystal formation (5), and the polymerization solidifies the crystalline arrangement of polyballs with minimum perturbation. Our results show that, by a change in gel composition, the filter can be tuned to reject different wavelengths, and the addition of sucrose improves the thermal stability of the CAF. The layer structures can be further exploited by stretching of the CAF to change the rejection wavelength (25).

REFERENCES AND NOTES

1. N. A. Clark, A. J. Hurd, B. J. Ackerson, *Nature* **281**, 57 (1979).
2. N. Ise, H. Matsuoka, K. Ito, *Z. Phys. Chem. Leipzig* **269**, 345 (1988); S. Dosho *et al.*, *Langmuir* **9**, 394 (1993).
3. P. Pieranski, *Contemp. Phys.* **24**, 25 (1983).
4. N. Ise, *Angew. Chem. Int. Ed. Engl.* **25**, 323 (1986).
5. R. H. Ottewill, *Langmuir* **5**, 4 (1989).
6. D. Thirumalai, *J. Phys. Chem.* **93**, 5637 (1989).
7. P. L. Flaugh, S. E. O'Donnell, S. A. Asher, *Appl. Spectrosc.* **38**, 847 (1984); T. Alfrey, E. B. Bradford, J. W. Vanderhoff, *J. Opt. Soc. Am.* **44**, 603 (1954); I. Amato, *Science* **255**, 1512 (1992).
8. H. P. Panzer, L. G. Magliocco, M. L. Cohen, W. S. Yen, European Patent 0 482 394 A2 (1992); corresponding U.S. patent pending.
9. Preliminary results of this investigation were presented to the Division of Colloid and Surface Science at the American Chemical Society's 204th national meeting, Washington, DC, 23 to 28 August 1992.
10. R. J. Spry and D. J. Kosan, *Appl. Spectrosc.* **40**, 782 (1986).
11. K. T. Tokuyasu, *J. Microsc.* **143**, 139 (1986).
12. J. Cohen *et al.*, *J. Colloid Interface Sci.* **156**, 137 (1993).
13. For description of the AAA notation, see, for example, A. Kelly and G. W. Groves, *Crystallography and Crystal Defects* (TechBooks, Fairfax, VA, 1970), chap. 3.
14. R. L. Hoffman, in *Science and Technology of Polymer Colloids*, G. W. Poehlein *et al.*, Eds. (NATO Advanced Study Institutes Series E, no. 68, Kluwer, Boston, MA, 1983), pp. 570–588.
15. I. M. Krieger, *ibid.*, pp. 523–530.
16. R. L. Hoffman, in *Future Directions in Polymer Colloids*, M. S. El-Aasser and R. M. Fitch, Eds. (NATO Advanced Study Institutes Series E, no. 138, Nijhoff, Boston, MA, 1987), pp. 151–165.
17. T. Weider *et al.*, *Phys. Rev. B* **47**, 5622 (1993); C. A. Murray and R. A. Wenk, *Phys. Rev. Lett.* **62**, 1643 (1989); C. A. Murray and D. H. Van Winkle, *ibid.* **58**, 1200 (1987); P. Richetti, J. Prost, P. Barois, *J. Phys. Paris* **45**, L1137 (1984); D. R. Nelson and B. I. Halperin, *Phys. Rev. B* **19**, 2457 (1979); G. Venkataraman and D. Sahoo, *Pramana* **24**, 317 (1985); J. D. Brock *et al.*, *Contemp. Phys.* **30**, 321 (1989).
18. B. J. Ackerson and N. A. Clark, *Phys. Rev. Lett.* **46**, 123 (1981).
19. D. H. Van Winkle and C. A. Murray, *J. Chem. Phys.* **89**, 3885 (1988).
20. B. J. Ackerson and N. A. Clark, in *Scattering Techniques Applied to Supramolecular and Nonequilibrium Systems*, S.-H. Chen *et al.*, Eds. (NATO Advanced Study Institutes Series B, no. 73, Plenum, New York, 1981), pp. 781–786.
21. M. Tomita and T. G. M. van de Ven, *J. Colloid Interface Sci.* **99**, 374 (1984).
22. P. Pieranski *et al.*, *Phys. Rev. Lett.* **50**, 900 (1983); D. H. Van Winkle and C. A. Murray, *Phys. Rev. A* **34**, 562 (1986).
23. N. Ise *et al.*, *Macromolecules* **22**, 1 (1989); N. Ise and T. Okubo, *Acc. Chem. Res.* **13**, 303 (1980); S. Ashdown *et al.*, *Langmuir* **6**, 303 (1990).
24. K. Ito *et al.*, *J. Am. Chem. Soc.* **110**, 6955 (1988); T. Yoshiyama and I. S. Sogami, *Langmuir* **3**, 851 (1987).
25. G. Haacke, H. P. Panzer, L. G. Magliocco, S. A. Asher, U.S. Patent 5 266 238 (1993).

26. E.A.K. acknowledges the assistance of S. Hardison in cryoultramicrotomy. Supported, in part, through an Air Force Wright research and development contract: prime contract no. F33615-88-C-5432 to S. Asher, subcontract 3382-1. We are grateful to S. Asher for the many fruitful discussions about this project.

13 July 1993; accepted 15 November 1993

Fossil Evidence for the Origin of Aquatic Locomotion in Archaeocete Whales

J. G. M. Thewissen, S. T. Hussain, M. Arif

Recent members of the order Cetacea (whales, dolphins, and porpoises) move in the water by vertical tail beats and cannot locomote on land. Their hindlimbs are not visible externally and the bones are reduced to one or a few splints that commonly lack joints. However, cetaceans originated from four-legged land mammals that used their limbs for locomotion and were probably apt runners. Because there are no relatively complete limbs for archaic archaeocete cetaceans, it is not known how the transition in locomotory organs from land to water occurred. Recovery of a skeleton of an early fossil cetacean from the Kuldana Formation, Pakistan, documents transitional modes of locomotion, and allows hypotheses concerning swimming in early cetaceans to be tested. The fossil indicates that archaic whales swam by undulating their vertebral column, thus forcing their feet up and down in a way similar to modern otters. Their movements on land probably resembled those of sea lions to some degree, and involved protraction and retraction of the abducted limbs.

The oldest cetacean, *Pakicetus*, is known from approximately 52-million-year-old river deposits in the Kuldana Formation in Pakistan (1, 2). We recovered several specimens of a new genus and species of cetacean, *Ambulocetus natans* (3) (Fig. 1), from lower to middle Eocene beds that are stratigraphically about 120 m higher than those that yielded *Pakicetus* in the Kala Chitta Hills. The best specimen is a partly articulated skull and skeleton of *Ambulocetus*. It was found in a silt and mudstone bed, scattered over an area of approximately 1.8 m^2 (4).

The same bed also contains impressions of leaves and abundant *Turritella* and other marine molluscs, indicating that the carcass was buried in a shallow sea. The holotype of *Ambulocetus* provides a glimpse of the transitional morphologies between four-legged whale ancestors (5, 6) and their finned descendants. Here, we focus on those morphological traits of *Ambulocetus* that have implications for locomotion in the earliest cetaceans.

Size of vertebrae, ribs, and limbs indicate that *Ambulocetus* was an archaeocete whale the size of a male of the sea lion *Otaria byronia* (approximately 300 kg). Cervical vertebrae are relatively long (centrum is 3 cm), and thoracic vertebrae have stout spinous processes and transverse processes with deeply excavated caudal sides. These depressions possibly gave rise to a strong spinal extensor muscle such as longissimus, which originates from the dorsal aspect of the transverse process in extant cetaceans (7, 8). The centrum of the only preserved lumbar vertebra is wide transversely and has large transverse processes but a weak spinous process. Spinal flexors and extensors originate from the transverse processes. Little is known about the tail, but there are always many caudal vertebrae in primitive cetaceans and their relatives (9), whereas the length of individual elements varies widely. The only caudal vertebra known for *Ambulocetus* is elongate, suggesting that the tail was much longer than in modern cetaceans.

Ambulocetus had a robust radius and ulna. The forearm was fixed in a semipronated position, as a result of the triangular shape of the radial head. The olecranon is strong and makes up one-third of the length of the ulna. It is inclined caudally, and would have allowed powerful elbow extension by triceps. Unlike modern cetaceans, elbow, wrist, and digital joints were flexible and synovial in *Ambulocetus*. The pisiform projects 4.5 cm from the wrist, and would have permitted

J. G. M. Thewissen, Department of Anatomy, Northeastern Ohio Universities College of Medicine, Box 95, Rootstown, OH 44272.
S. T. Hussain, Department of Anatomy, College of Medicine, Howard University, Washington, DC 20059.
M. Arif, Stratigraphy/Paleontology Branch, Geological Survey of Pakistan, 84 H-8/1, Islamabad, Pakistan.